GSA Data Repository item 2019136
Sizemore, T. Wielicki, M.M., Çemen, I., Stockli, D., Heizler, M., and Robinson, D., 2019, Structural evolution of central Death Valley, California, using new thermochronometry of the Badwater turtleback: Lithosphere, https://doi.org/10.1130/L1044.1

**Sample Selection and Methods**

Our transect route was chosen based on what we determined to be the maximum exposure of basement gneiss (containing the requisite minerals for thermochronometry) and the feasibility of navigating the terrain on foot. Samples were extracted from in-situ outcrops at approximately 200-meter elevation intervals and geo-located using a handheld GPS. We avoided collecting samples near dikes or obvious fault rocks.

Samples were brought back to the University of Alabama, photographed, and crushed using a jaw crusher and disk mill. We used a rare-Earth magnet and Frantz magnetic separator to remove the magnetic minerals from the 62-250 micron fraction. We separated the fraction by density using Bromoform and methylene iodide. We handpicked zircon, apatite, and K-feldspar from the final separates while targeting clean, euhedral grains with no inclusions or other defects. Muscovite and biotite were handpicked from the coarsely crushed sample.

For U-Pb analysis, we selected ten zircon grains from each of the Willow Springs diorite, the Smith Mountain granite, and the gneissic sample S-795 (corresponding to elevation in meters). The grains, together with AS3 zircon standard, were mounted into clear, one-inch epoxy mounts and polished to expose the cores of the grains. We then examined the grains for inclusions and defects and imaged them using a scanning electron microscope with energy-dispersive x-ray spectroscopy. Secondary ion microprobe analyses were conducted using the CAMECA ims1270 at the University of California, Los Angeles, using an ~8-12 nA mass-filtered $^{16}O$ beam focused to spots between ~20-35 micrometers (Williams et al., 1984; Paces and Miller, 1993). A 91500 zircon was used as a primary standard for U and Th concentrations. All but 4 of the grains from the Willow Springs diorite were too fractured or small for suitable analysis.

For (U-Th)/He analysis, we selected four to five zircon and apatite grains from each sample that were, in general, ≥70 μm in width, which we then measured and photographed using a high-powered, cross-polarized stereographic microscope with a rotating stage and a mounted digital camera. This technique was used in an attempt to minimize errors associated with alpha-ejection (Ft) correction and trace-element contamination as described in Farley et al. (1996). Individual grains were packed into 1-mm Pt foil tubes and crimped on both ends. Apatite grains were heated for 5 minutes at 1070°C using a continuous-mode Nd-YAG laser whereas zircon grains were heated for 10 minutes at 1300°C. We extracted and measured $^{4}He$ gas from the individual grains using an ultra-high vacuum noble gas extraction and purification line with two Blazers Prisma QMS-200 quadrupole mass spectrometers. The line was spiked with $^{3}He$ for calibration. We used four zircon standards from

the Fish Canyon Tuff (U-Th/He age of 27.8 ± 0.8 Ma; see summary in Villeneuve et al., 2000) and four apatite standards of Durango apatite (U-Th/He age of 31.9 ± 0.5 Ma; Young et al., 1969; McDowell and Keizer, 1977, Farley, 2000). Apatite grains were digested in their Pt foil tubes in $^{230}$Th, $^{235}$U, and $^{149}$Sm spiked $HNO_3$ solution. Zircon grains were degassed after removal them from the Pt foil tubes and being dissolved using the standard Parr pressure vessel digestion procedure utilizing HF-$HNO_3$ and HCL. We then analyzed all dissolved grains for U, Th, and Sm using a Thermo-Scientific Element-2 inductively coupled plasma mass spectrometer (ICP-MS).

For Ar/Ar analysis, coexisting biotite, muscovite, and K-feldspar were analyzed from samples S-1278 and S-971. Due to compositional differences in the lower-elevation samples, only K-feldspar was analyzed in sample S-448, only muscovite and K-feldspar were analyzed in sample S-193, and only biotite was analyzed in sample S-62. Mineral separates were loaded into machined aluminum disks and irradiated for 8 hours in the central thimble, Triga Reactor, United States Geological Survey (USGS) at Denver, Colorado. We used the Fish Canyon Tuff sanidine (FC-2) as a neutron flux monitor with an assigned age of 28.201 Ma (Kuiper et al., 2008).

Isotopic analysis was conducted using a Thermo Scientific Helix MC mass spectrometer online with an automated all-metal extraction system. K-feldspar and muscovite were step-heated in a Nb resistance furnace from 5 - 121 minutes. Reactive gasses were removed during heating with a SAES GP-50 getter operated at ~450°C. Additional cleanup was conducted in a second stage for one minute with a SAES GP-50 getter operating at ~450°C. Biotite was step-heated using 40 seconds per step with a 55W Photon-Machines diode laser. The reactive gasses were removed by a 1-minute reaction with a SAES GP-50 getter operated at 450°C and gas was also exposed to a cold finger operated at -140°C.

**Calculation Details and Error Reporting**

For the U-Pb analysis, data reduction and calculation of U–Pb ages were done using the UCLA software (ZIPS v3.0.4 by C.D. Coath, internal unpublished software) and Isoplot v.4.15 (Ludwig, 2008). Error was calculated using the method of Stern and Amelin (2003).

For the (U-Th)/He analysis, we used the standard practice of apply a 6% error to single-grain apatite ages and 8% to single-grain zircon ages. These percentage errors are based on the reproducibility of laboratory standards (Farley et al., 2001; Reiners et al., 2002; Tables A1-A4). We report the error for our mean ages as the standard deviation (1$\sigma$) of the aliquots for a sample (Tables A3-A4). Tables A1 and A2 summarize our (U-Th)/He mean ages along with associated errors (1$\sigma$). In each sample we used three or more replicates to calculate our mean ages. Some aliquot ages were excluded from our calculations as outliers, which included either ages that were more

than 2 standard deviations from the mean or anomalously low concentrations of U, Th, and Sm compared to other grains. The former criterion was likely caused by the presence of mineral or fluid inclusions within the grain and potentially "parentless" helium (House et al., 1999). In addition, we screened the data for evidence of radiation damage effects by looking for a strong positive or negative correlation between the aliquot ages and both U and He concentration (Nasdala et al., 2004; Reiners, 2005; Shuster et al., 2006; Flowers et al., 2009; Guenthner et al., 2013), but did not identify any radiation damage effects.

For the Ar/Ar analysis, we corrected isotopic ratios for blank, radioactive decay, and mass discrimination, but not for interfering reactions. Errors quoted for individual analyses include analytical error only, without interfering reaction or J uncertainties. We calculated integrated age by summing isotopic measurements of all steps. We calculated integrated age error by quadratically combining errors of isotopic measurements of all steps. The plateau age is the inverse-variance-weighted mean of all selected steps. The plateau age error is the inverse-variance-weighted mean error (Tayor, 1972) times root MSWD where MSWD>1. We reported isotopic abundances of Steiger and Jäger (1977). Detector intercalibration is measured $^{40}Ar/^{39}Ar$ divided by 295.5. The weight percent $K_2O$ is calculated from $^{39}Ar$ signal, sample weight, and instrument sensitivity. All ages are calculated relative to FC-2 Fish Canyon Tuff sanidine interlaboratory standard at 28.201 Ma. We used the K decay constant of 5.453xe-10/year and the following correction factors: $(^{39}Ar/^{37}Ar)Ca = 0.0007115 \pm 9e\text{-}6$, $(^{36}Ar/^{37}Ar)Ca = 0.0002755 \pm 1e\text{-}6$, $(^{40}Ar/^{39}Ar)K = 0.0088 \pm 0.0004$.

## REFERENCES CITED


Farley, K.A., Wolf, R.A., and Silver, L.T., 1996, The effects of long alpha-stopping distances on (U-Th)/ He ages: Geochimica et Cosmochimica Acta, v. 60, p. 4223–4229, doi:10.1016/S0016-7037(96)00193-7.

Farley, K.A., 2000, Helium diffusion from apatite: General behavior as illustrated by Durango fluorapatite: Journal of Geophysical Research: Solid Earth, v. 105, p. 2903–2914, doi: 10.1029/1999JB900348.

Farley, K.A., Rusmore, M.E., and Bogue, S.W., 2001, Exhumation and uplift history of the central Coast Mountains, British Columbia, from apatite (U-Th)/He Thermochronometry: Geology, v. 29, p. 99–102, doi:10.1130/0091-7613(2001)029<0099:PMUAEO>2.0.CO;2.

Flowers, R.M., Ketcham, R.A., Shuster, D.L., and Farley, K.A., 2009, Apatite (U-Th)/He thermochronometry using a radiation damage accumulation and annealing model: Geochimica et Cosmochimica Acta, v. 73, p. 2347–2365, doi:10.1016/j.gca.2009.01.015.

Guenthner, W., Reiners, P.W., Ketcham, R.A., Nasdala, L., and Giester, G., 2013, Helium diffusion in natural zircon: Radiation damage, anisotropy, and the interpretation of zircon (U-Th)/He thermochronology: American Journal of Science, v. 313, p. 145–198, doi:10.2475/03.2013.01.

House, M.A., Farley, K.A., and Kohn, B.P., 1999, An empirical test of helium diffusion in apatite; borehole data from the Otway Basin, Australia: Earth and Planetary Science Letters, v. 170, p. 463–474, doi:10.1016/S0012-821X(99)00120-X.

Kuiper, K.F., Deino, A., Hilgen, F.J., Krijgsman, W., Renne, P.R., and Wijbrans, J.R., 2008, Synchronizing Rock Clocks: v. 320.

Ludwig, K.R., 2008. User's Manual for Isoplot 3.70, a Geochronological Toolkit for Microsoft Excel: Berkeley Geochronological Center, Special Publication No. 4. pp. 1–76.

McDowell, F.W., and Keizer, R., 1977, Timing of mid-tertiary volcan- ism in the Sierra Madre Occidental between Durango City and Mazatlan, Mexico: Geol. Soc. Amer. Bull., v. 88, p. 1479–1486.

Nasdala, L., Reiners, P.W., Garver, J.I., Kennedy, A.K., Stern, R.A., Balan, E., and Wirth, R., 2004, Incomplete retention of radiation damage in zircon from Sri Lanka: The American Mineralogist, v. 89, p. 219–231.

Paces, J.B., and Miller, J.D., 1993, Precise U-Pb ages of Duluth Complex and related mafic intrusions, northeastern Minnesota: Geochronological insights to physical, petrogenetic, paleomagnetic, and tectonomagmatic processes associated with the 1.1 Ga Midcontinent Rift System: Journal of Geophysical . Research, v. 98(B8), p. 13997–14013, doi: 10.1029/93JB01159.

Reiners, P.W., 2005, Zircon (U-Th)/He Thermochronometry, in Reiners, P.W. and Ehlers, T.A. eds., Thermochronology, Reviews in Mineralogy and Geochemistry, v. 58, p. 151–176.

Reiners, P.W., Farley, K.A., and Hickes, H.J., 2002, He diffusion and (U-Th)/He thermochronometry of zircon: Initial results from Fish Canyon Tuff and Gold Butte: Tectonophysics, v. 349, p. 297–308, doi:10.1016/S0040-1951(02)00058-6.

Shuster, D.L., Flowers, R.M., and Farley, K.A., 2006, The influence of natural radiation damage on helium diffusion kinetics in apatite: Earth and Planetary Science Letters, v. 249, no. 3–4, p. 148–161, doi:10.1016/j.epsl.2006.07.028.

Steiger R.J., Jäger E., 1977, Subcommission on geochronology: Convention on the use of decay constants in geo-

and cosmocchronology: Earth Planet. Sci. Lett., v. 36, p. 359-362.

Stern, R.A., Amelin, Y., 2003, Assessment of errors in SIMS zircon U–Pb geochronology using a natural zircon standard and NIST SRM 610 glass: Chemical Geology, v. 197, no. 1-4, p. 111-143.

Taylor, J.R., 1982, An Introduction to Error Analysis: the Study of Uncertainties in Physical Measurements: University Science Books, Mill Valley, CA, p. 270.

Villeneuve, M., Sandeman, H.A., and Davis, W.J., 2000, A method for intercalibration of U-Th-Pb and40Ar-39Ar ages in the Phanerozoic: Geochimica et Cosmochimica Acta, v. 64, p. 4017–4030, doi: 10.1016/S0016-7037(00)00484-1.

Young, E.J., Myers, A.T., Munson, E.L., and Conklin, N.M., 1969, Mineralogy and geochemistry of fluorapatite from Cerro de Mercado, Durango, Mexico: U.S. Geol. Surv. Prof. Pap. 650-D, D84–D93.

Williams, I.S., Compston, W., Black, L.P., Ireland, T.R., and Foster, J.J., 1984, Unsupported radiogenic Pb in zircon: a cause of anomalously high Pb-Pb, U-Pb and Th-Pb ages: Contributions to Mineralogy and Petrology, v. 88, p. 322–327, doi: 10.1007/BF00376756.

See also Tables DR1 - DR8 in the companion file, 2019136.xlsx, and the sample locations in 2019136.kmz.

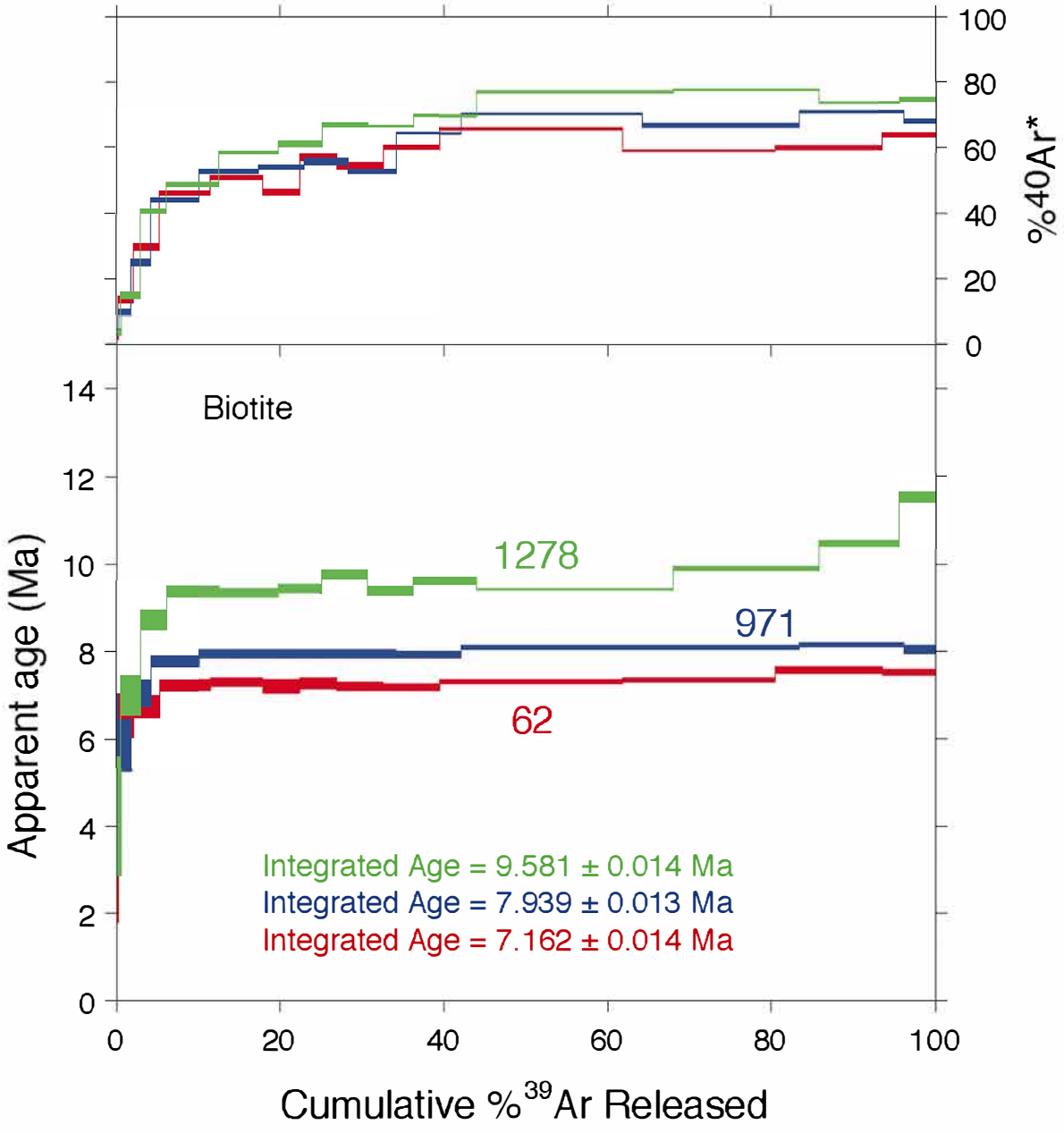


Figure DR1. Biotite argon release spectra and age results for S-62, S-971, and S-1278.

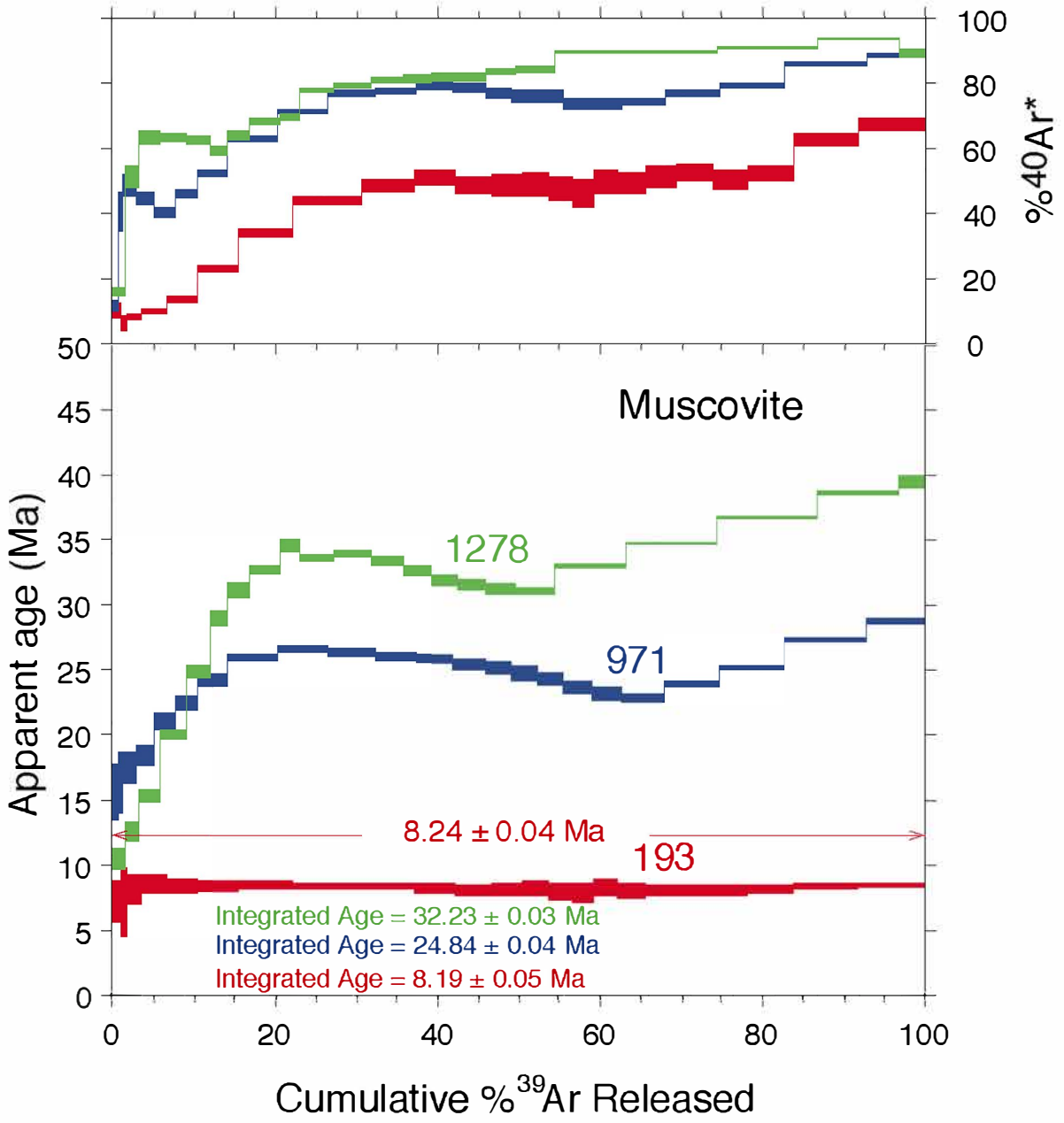


Figure DR2. Muscovite argon release spectra and age results for S-193, S-971, and S-1278.

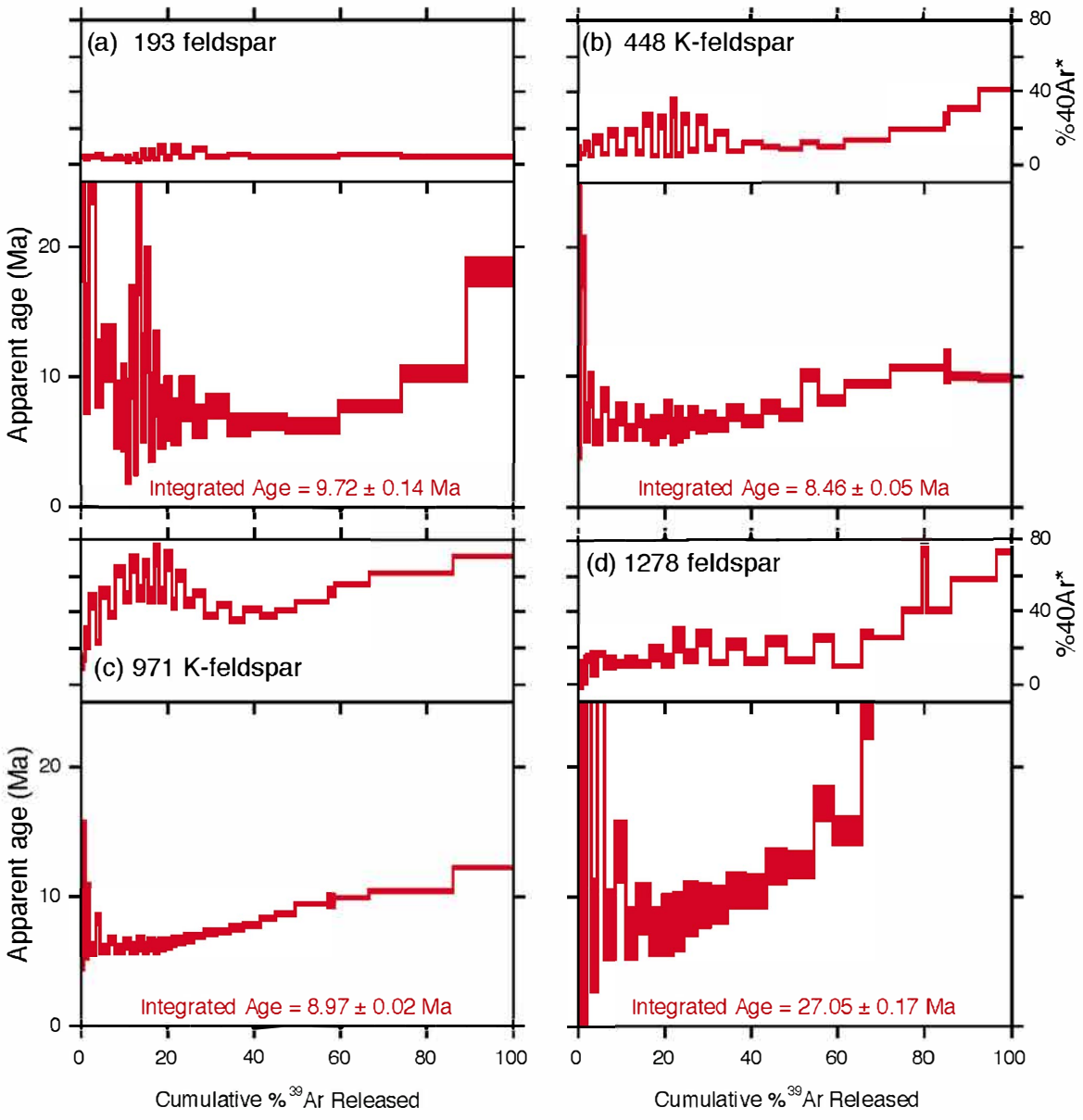


Figure DR3. K-feldspar argon release spectra and age results for S-193, S-448, S-971, and S-1278.

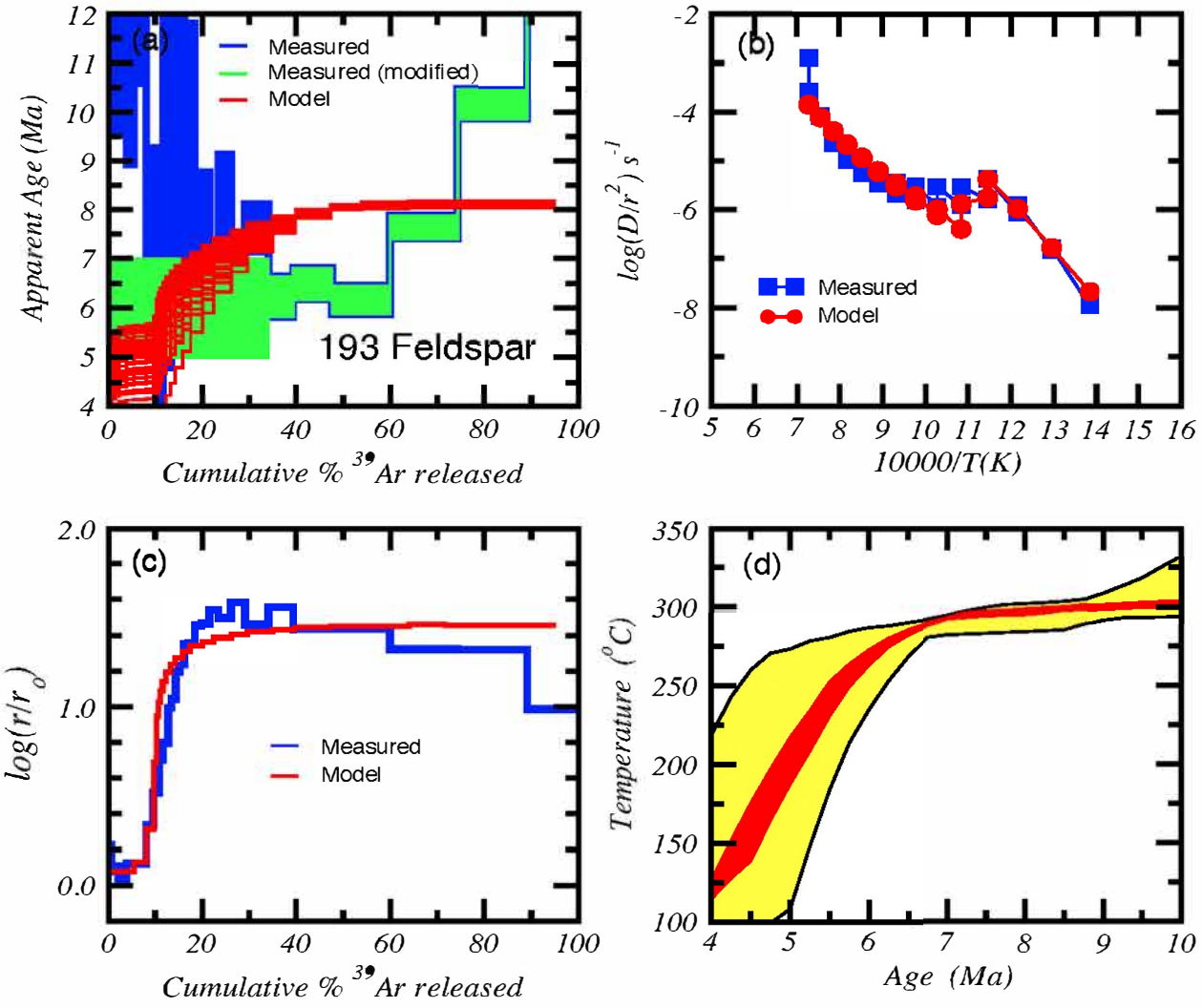


Figure DR4. Multi-domain diffusion modeling results for S-193 feldspar. A: Argon release spectra and measured age during step-heating; B: Arrhenius plot for measured and modeled argon diffusion; C: Measured and modeled $\log(r/r_0)$ versus cumulative $\%^{39}Ar$ released; D: Model output showing temperature versus age envelope (red=1-sigma, yellow=2-sigma).

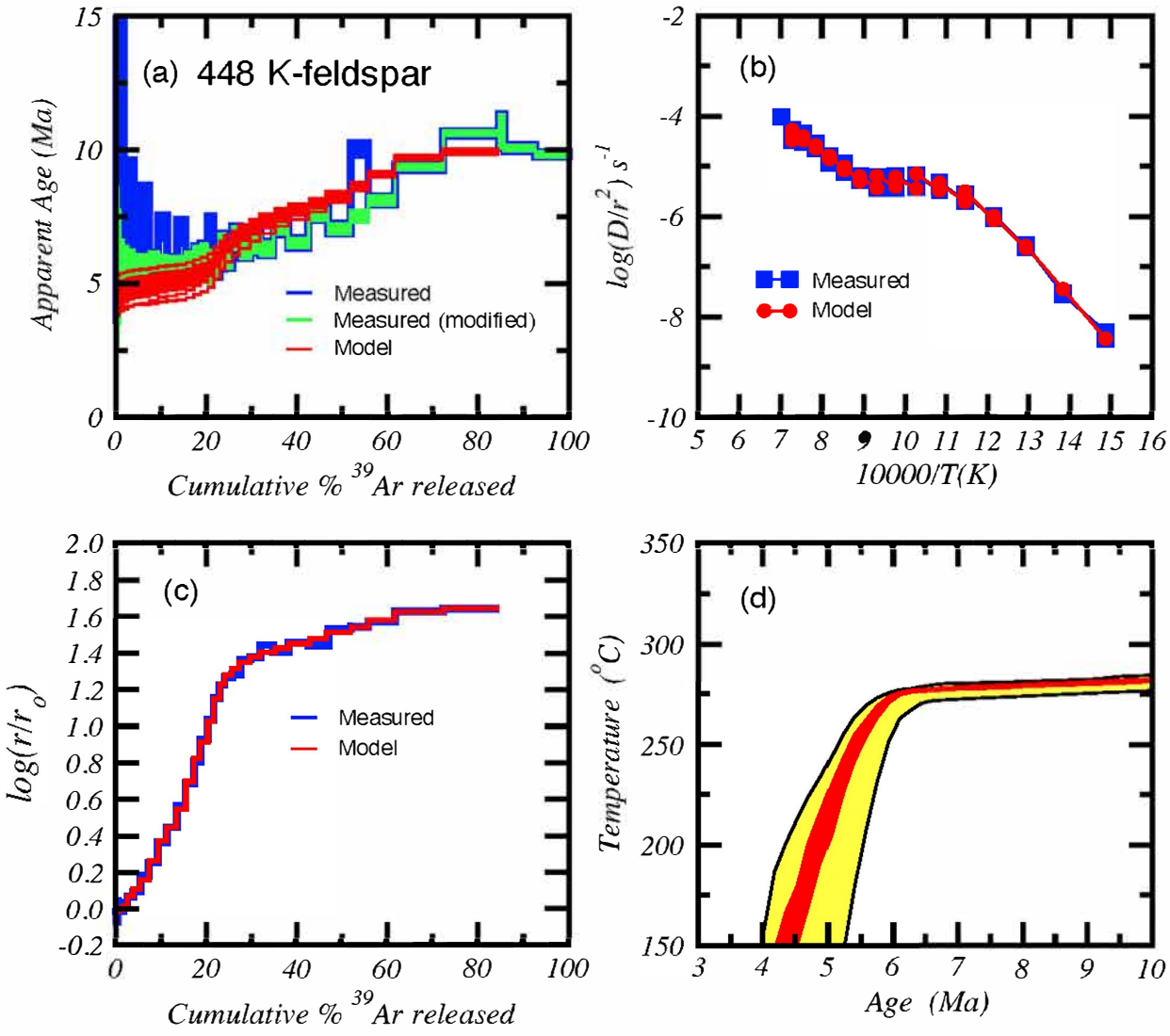


Figure DR5. Multi-domain diffusion modeling results for S-448 K-feldspar. A: Argon release spectra and measured age during step-heating; B: Arrhenius plot for measured and modeled argon diffusion; C: Measured and modeled $\log(r/r_0)$ versus cumulative $\%^{39}Ar$ released; D: Model output showing temperature versus age envelope (red=1-sigma, yellow=2-sigma).

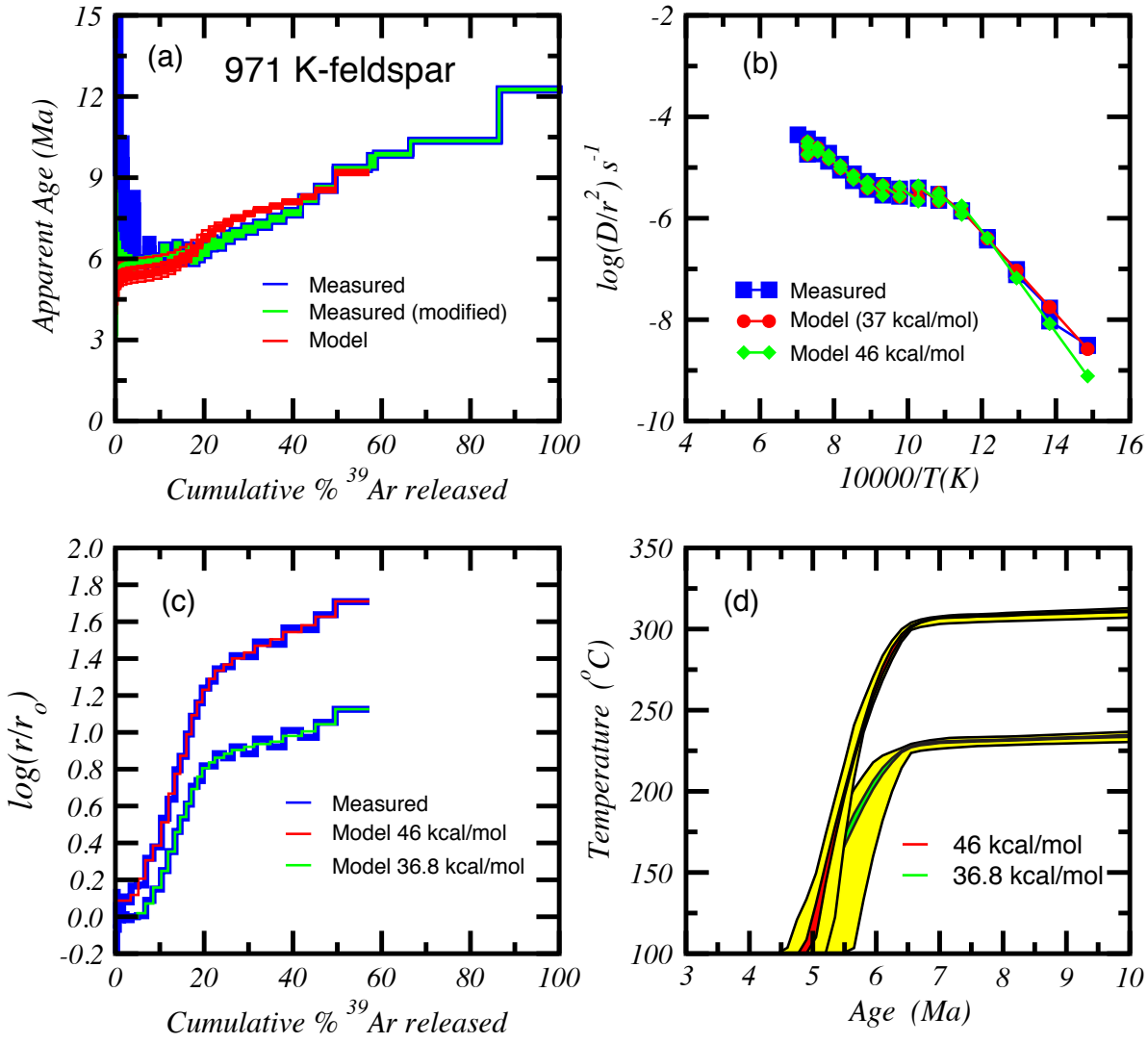


Figure DR6. Multi-domain diffusion modeling results for S-971 K-feldspar. A: Argon release spectra and measured age during step-heating; B: Arrhenius plot for measured and modeled argon diffusion; C: Measured and modeled log(r/r0) versus cumulative %39 Ar released; D: Model output showing temperature versus age envelope (red=l-sigma, yellow/ green=2-sig-ma).

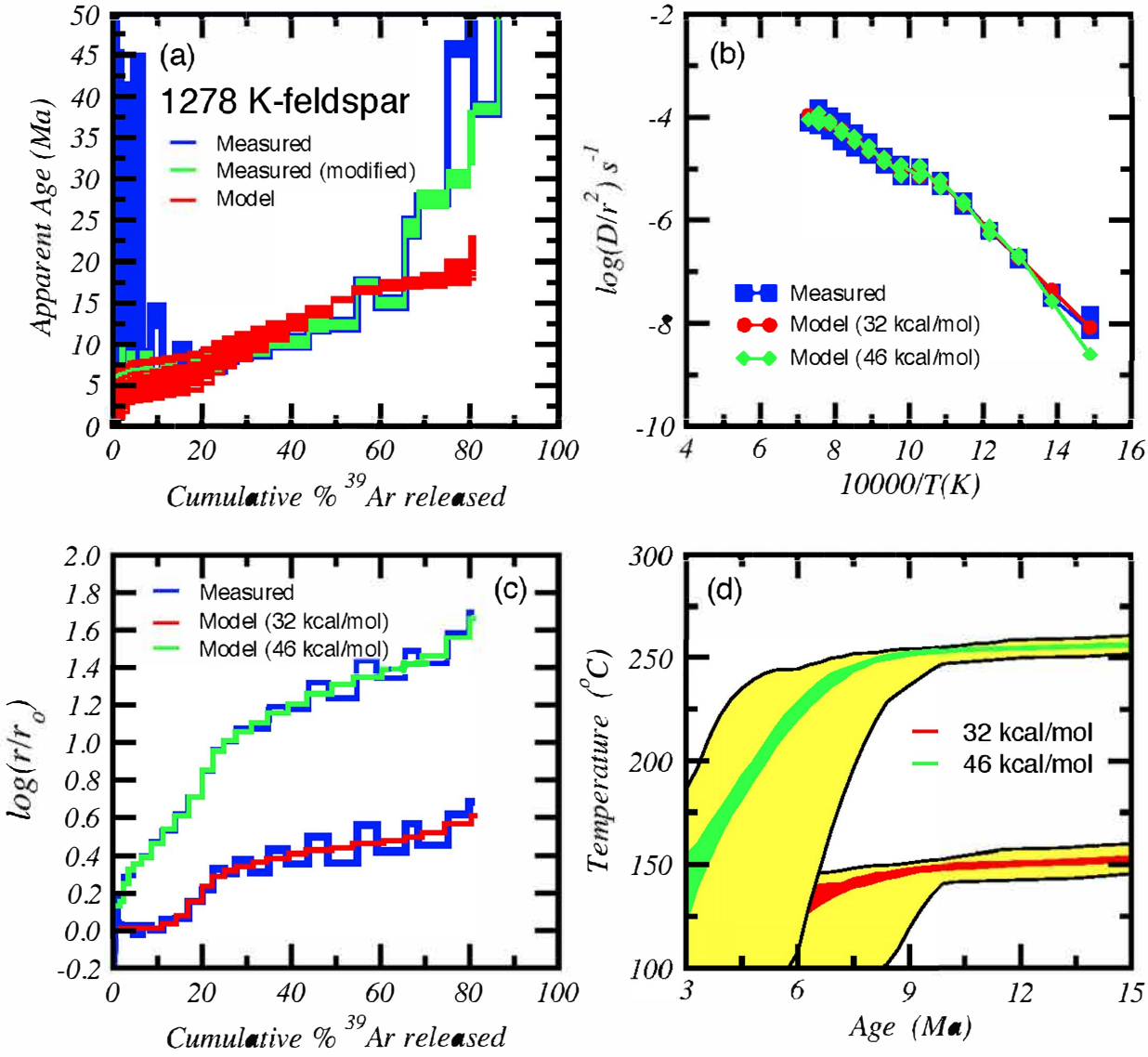


Figure DR7. Multi-domain diffusion modeling results for S-1278 K-feldspar. A: Argon release spectra and measured age during step-heating; B: Arrhenius plot for measured and modeled argon diffusion; C: Measured and modeled log(r/$r_0$) versus cumulative %$^{39}$Ar released; D: Model output showing temperature versus age envelope (red=1-sigma, yellow/green=2-sigma).

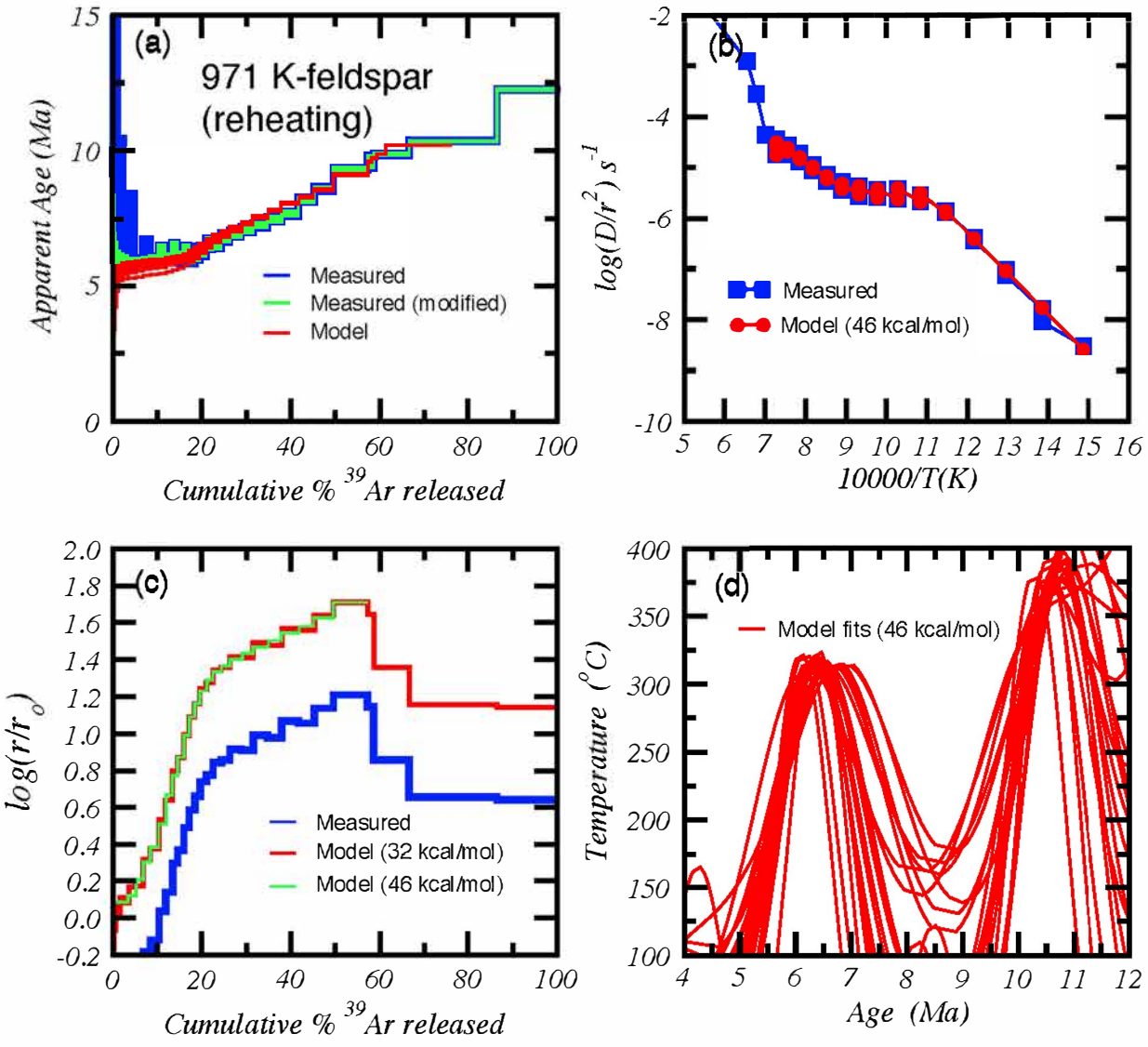


Figure DR8. Multi-domain diffusion modeling results for S-971 K-feldspar with a simulated reheating event at ca. 6.5 Ma. A: Argon release spectra and measured age during step-heating; B: Arrhenius plot for measured and modeled argon diffusion; C: Measured and modeled $\log(r/r_0)$ versus cumulative $\%^{39}Ar$ released; D: Model output showing model fits temperature versus age compatible with reheating event.

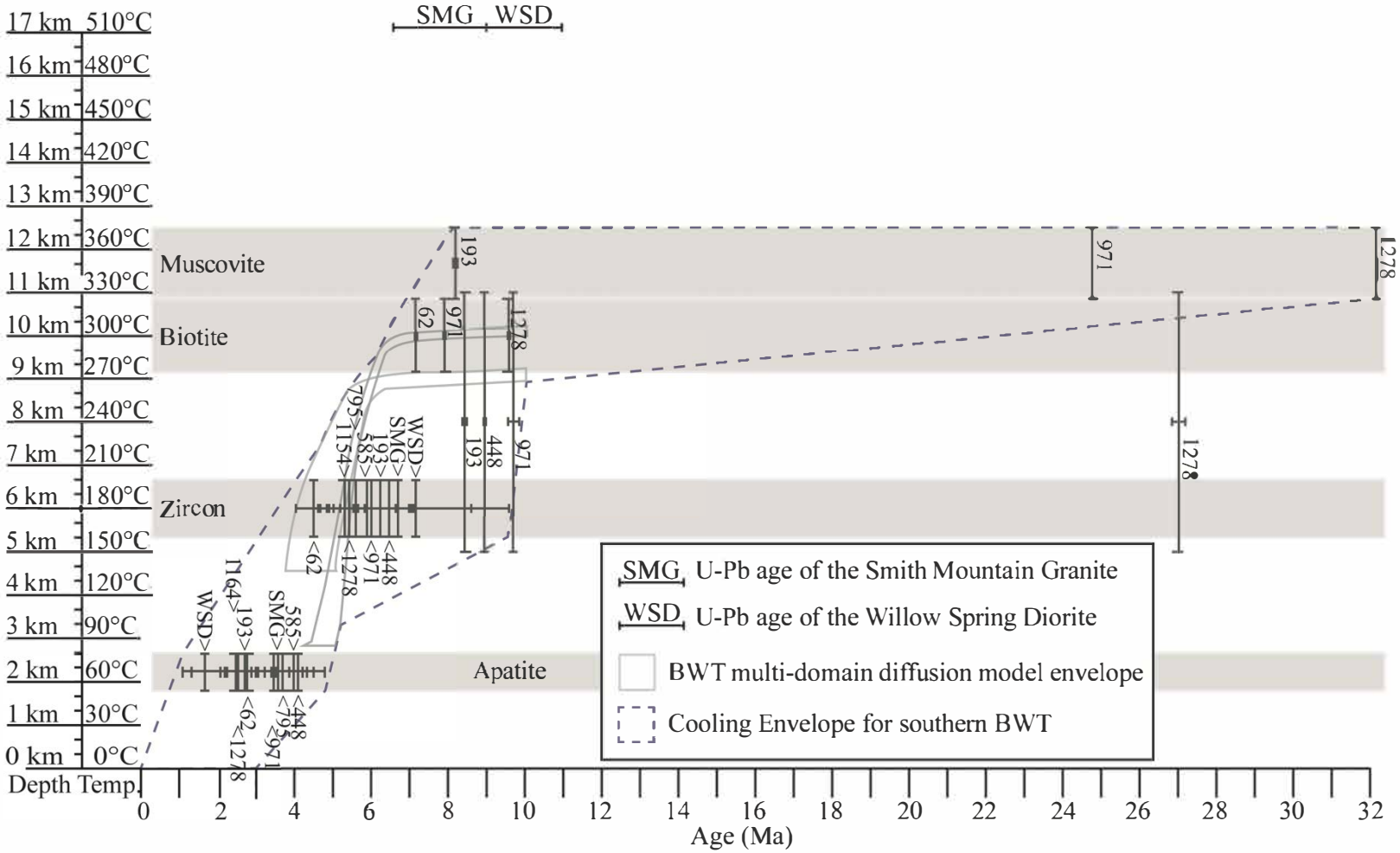


Figure DR 9. Raw data used to create cooling envelope for the Badwater turtleback (BWT), and crystallization ages (this study) of the adjancent Smith Mountain Granite (SMG) and Willow Spring Diorite (WSD). Number labels on plot correspond to sample elevation. Horizontal grey boxes and vertical error bars indicate closure temperatures of each system (see text for details). Horizontal error bars indicate calculated cooling age error. Raw K-feldspar cooling ages were excluded from envelope due to high uncertainty in closure temperature. Depth and exhumation rates on the Y-axis are based on a 30°C/km geothermal gradient, which is evidened by thermokinematic modeling by Bidgoli et al., 2015.

Bidgoli, T.S., Amir, E., Walker, J.D., Stockli, D.F., Andrew, J.E., and Caskey, S.J., 2015, Low-temperature thermochronology of the Black and Panamint mountains, Death Valley, California: Implications for geodynamic controls on Cenozoic intraplate strain: Lithosphere, v. 7, p. 473–480, https://doi.org/10.1130/L406.1.